**Atmospheric
Chemistry
and Physics
Discussions**

The effects of timing and rate of marine cloud brightening aerosol injection on albedo changes during the diurnal cycle of marine stratocumulus clouds

A. K. L. Jenkins, P. M. Forster, and L. S. Jackson

School of Earth and Environment, University of Leeds, Leeds, UK

Correspondence to: A. K. L. Jenkins (eeaklj@leeds.ac.uk)

The effects of marine cloud brightening aerosol injection on albedo changes

A. K. L. Jenkins et al.

Title Page	
Abstract	Introduction
Conclusions	References
Tables	Figures
◄◄	►►
◄	►
Back	Close

Full Screen / Esc

Printer-friendly Version

Interactive Discussion

Abstract

The marine-cloud brightening geoengineering technique has been suggested as a possible means of counteracting the positive radiative forcing associated with anthropogenic atmospheric CO_2 increases. The focus of this study is to quantify the albedo response to aerosols injected into marine stratocumulus cloud from a point source at different times of day. We use a cloud-resolving model to investigate both weakly precipitating and non-precipitating regimes. Injection into both regimes induces a first indirect aerosol effect. Additionally, the weakly precipitating regime shows evidence of the second indirect aerosol effect and leads to cloud changes indicative of a regime change to more persistent cloud. This results in a cloud albedo increase up to six times larger than in the non-precipitating case. These indirect effects show considerable variation with injection at different times in the diurnal cycle. For the weakly precipitating case, aerosol injection results in average increases in cloud albedo of 0.28 and 0.17 in the early and mid morning (03:00:00 local time (LT) and 08:00:00 LT, respectively) and 0.01 in the evening (18:00:00 LT). No cloud develops when injecting into the cloud-free day (13:00:00 LT). However, the all-sky albedo increases (which include both the indirect and direct aerosol effects) are highest for early morning injection (0.11). Mid-morning and daytime injections produce increases of 0.06, with the direct aerosol effect compensating for the lack of cloud albedo perturbation during the cloud-free day. Evening injection results in an increase of 0.04. Penetration and accumulation of aerosols above the cloud top may lead to a reduction of all-sky albedo that tempers the cloud albedo increases. The apparent direct aerosol tempering effect increases with injection rate, although not enough to overcome the increase in all-sky planetary albedo resulting from increases in cloud albedo. For the weakly precipitating case considered, the optimal injection time for planetary albedo response is the early morning. Here, the cloud has more opportunity develop into a more persistent non-precipitating regime prior to the dissipative effects of solar heating. The effectiveness of the sea-spray injection method is highly sensitive to diurnal injection time and the direct aerosol effect of an

intense aerosol point source. Studies which ignore these factors could overstate the effectiveness of the marine cloud brightening technique.

1 Introduction

Geoengineering schemes have been proposed that decrease the amount of solar ra-
diation reaching the Earth's surface, creating a cooling effect that could potentially
ameliorate future greenhouse gas driven warming (Lenton and Vaughan, 2009). One
such scheme, the marine-cloud brightening geoengineering proposal (Latham, 1990,
2002), aims to brighten low cloud, generating a negative radiative forcing from the
cloud albedo increase. The original proposal assumed that this albedo increase could
be achieved by the deliberate enhancement of the indirect aerosol effect through the
injection of aerosols into the marine boundary layer from unmanned wind-powered
vessels (Salter et al., 2008).

Marine cloud brightening has been simulated in both Global Circulation Models
(GCMs) and higher resolution cloud-resolving models. GCMs have difficulty represent-
ing an aerosol point source but are able to simulate the large-scale response of the
atmosphere and ocean (when combined with an ocean model). First investigations in-
creased the cloud droplet number concentrations (N_d) for low-level clouds to a fixed
value of $375\,\mathrm{cm^{-3}}$ and found forcings ranged from $-0.97\,\mathrm{W\,m^{-2}}$ for three regions of
persistent marine stratocumulus (Jones et al., 2009) to $-8.0\,\mathrm{W\,m^{-2}}$ for adjustment of
all low-level maritime cloud (Latham et al., 2008). These simulations also found signifi-
cant regional climate change that was not offset and also found varying sensitivities of
different climate variables (Rasch et al., 2009). For example, precipitation decreases of
up to $1\,\mathrm{mm\,day^{-1}}$ have been simulated in the Amazon when cloud drop concentrations
were changed (Jones et al., 2009, 2011a).

Global aerosol and climate-aerosol model simulations moved away from the fixed
assumed N_d, basing the input aerosol injection rates on design characteristics of the
proposed wind-powered sea-water spray pumping vessels (Salter et al., 2008). These

The effects of marine cloud brightening aerosol injection on albedo changes

A. K. L. Jenkins et al.

Title Page

Abstract	Introduction
Conclusions	References
Tables	Figures

◄ | ►|

◄ | ►

Back | Close

Full Screen / Esc

Printer-friendly Version

Interactive Discussion

simulations resulted in maximum N_d of 177 cm^{-3} (Korhonen et al., 2010) and 286 cm^{-3} (Partanen et al., 2012) in the injected regions. Based on similar injection areas as Jones et al. (2009), Partanen et al. (2012) calculated a global mean radiative forcing of −0.8 W m^{-2} which included a −0.1 W m^{-2} direct aerosol effect, resulting largely from areas of low cloud cover. Whilst the increasingly complex global models are able to represent interactions between injected aerosols, background aerosols, clouds and the climate, large uncertainties remain, especially at the cloud process scale (Wang and Feingold, 2009a,b). Aerosol injection processes and marine stratocumulus (MSc) dynamical processes occur at scales of tens of meters, and therefore can only be examined in detail using cloud-resolving models.

Using a cloud-resolving large-eddy simulation (LES), Wang et al. (2011) found that the albedo response to aerosol injection is regime dependent. Heavy precipitation largely scavenging out the injected aerosol, whilst heavily polluted clouds showed little albedo change owing to the already high albedo. Dry regimes offset increased N_d with losses from increased evaporation of the smaller particles. Only weakly precipitating regimes and low CCN conditions (possibly following heavy precipitation) were effectively altered by aerosol injection. Point source injection of aerosols was found to induce complex dynamical feedbacks in precipitating regimes – associated with the buffered-system nature of clouds (Stevens and Feingold, 2009) – and a spatially inhomogeneous albedo response. This small-scale inhomogeneity deviates from the inherent uniformity of both aerosol injection and cloud response of global scale models.

The diurnal cycle of MSc in GCMs is produced using a parameterisation of entrainment. The simulated diurnal cycle is thus sensitive to the performance of the parameterisation (Lock, 2004). The diurnal cycle of MSc in cloud-resolving models is produced through the explicit handling of physical processes, and thus is not prone to problems associated with the parameterised representations. The MSc diurnal cycle is caused by short-wave (SW) solar insolation. The resulting SW in-cloud warming offsets the long-wave (LW) cloud-top radiative cooling and therefore reduces the turbulence that sustains the cloud (Nieuwstadt and Duynkerke, 1996; Duynkerke and Teixeira, 2001;

Title Page

Abstract	Introduction
Conclusions	References
Tables	Figures

◀◀ ▶▶

◀ ▶

Back Close

Full Screen / Esc

Printer-friendly Version

Interactive Discussion

Duynkerke et al., 2004). MSc therefore typically exhibit decoupling of the cloud and sub-cloud layers and cloud dissipation during daylight. The extent of this is dependent on conditions, but is evident in losses in both cloud liquid water path (LWP) and cloud fraction (Duynkerke and Teixeira, 2001; Bretherton et al., 2004; Duynkerke et al., 2004). As the warming effect of the SW radiation stops during the night, the cloud can recover (Wang et al., 2010). Hence, in addition to the range of cloud conditions produced by background atmospheric and background aerosol conditions, further variation will occur through the diurnal cycle. Cloud-resolving simulations of the effects of aerosol injection into different cloud conditions have assumed repeated aerosol injection throughout the day (Wang et al., 2011) and have not investigated the effect of timing of aerosol injection during the diurnal cycle on planetary albedo change effectiveness.

This study investigates the efficacy of aerosol injection on both cloud albedo and all-sky albedo increases, with injection at different times in the diurnal cycle, and at three different aerosol injection rates. The effect is quantified for both weakly precipitating (WP) and non-precipitating (NP) regimes. From this, the optimal time of day to inject aerosols is identified.

The effect of the very high local concentrations of aerosol caused by point source injection on albedo is also considered. We quantify the contribution of the direct aerosol effect and how this direct effect interacts with the indirect effect associated with changes in cloud albedo.

2 Model set-up

We use the Weather Research and Forecasting model coupled with Chemistry (WRF/Chem) V3.3.1 (Skamarock et al., 2008) in the large-eddy simulation (LES) configuration. This model incorporates interactive chemistry through the Carbon Bond Mechanism – Z (CBMZ) gas phase chemical mechanism scheme (Zaveri and Peters, 1999; Fast et al., 2006) and aerosol processes through the 8-bin MOSAIC scheme (Zaveri et al., 2008). Aerosols interact with the cloud through the Morrison et al. (2005)

two-moment microphysics scheme. Activation of aerosols to cloud droplets follows the Abdul-Razzak and Ghan (2000) method. LW radiation calculations were performed by the CAM spectral-band LW scheme (Collins et al., 2004). SW radiation calculations were performed by the RRTMG transfer scheme. The 1.5 order 3-D turbulent kinetic energy closure scheme (Skamarock et al., 2008) was utilised to simulate sub-grid turbulence. Advection was constrained by the monotonic flux limiter option (Wang et al., 2009). Surface layer physical processes were represented by the Monin-Obukov scheme. Horizontal boundary conditions were periodic, and a 250 m damping layer was included at the model top. Subsidence was included through a large-scale horizontal divergence of $3.75 \times 10^{-6} \, \text{s}^{-1}$. Large-scale wind was initialised at zero (following Wang and Feingold, 2009a; Wang et al., 2011).

Input soundings follow Research Flight 02 (RF02) of the DYCOMS-II field campaign which observed drizzling stratocumulus (Ackerman et al., 2009). The inversion height was 795 m. Total water mixing ratio was initialised at $9.45 \, \text{g kg}^{-1}$ in the boundary layer, decreasing to $5.0 \, \text{g kg}^{-1}$ in the free troposphere. The potential temperature was initialised to 288.3 K in the boundary layer, increasing to 303.9 K by 1500 m height.

Three background aerosol concentration initialisations for SO_4, NH_4, NO_3, Na, Cl, black carbon and organic carbon, obtained from model output of the global atmospheric aerosol and chemistry GLOMAP model (Mann et al., 2010), were selected to reproduce cloud properties under a range of background marine aerosol concentrations. The three representative aerosol locations chosen were: the Southern Ocean, a pristine case; the North-East Pacific, the location of the Second Dynamics and Chemistry of Marine Stratocumulus (DYCOMS-II) mission (Stevens et al., 2003) and an area of persistent MSc cloud; and the East China Sea, an area of high atmospheric aerosol concentration resulting from mainly anthropogenic sources.

The background aerosol budget comprised a natural wind-driven sea-spray source (Fuentes et al., 2010); activation of background and emitted gases; and a wet deposition sink. The gases SO_2, H_2O_2, NH_3, CO and O_3 were initialised with values typical of the oceanic boundary layer atmosphere in regions of MSc (Georgii and Gravenhorst,

Title Page

Abstract	Introduction
Conclusions	References
Tables	Figures

◄◄	►►
◄	►
Back	Close

Full Screen / Esc

Printer-friendly Version

Interactive Discussion

1977; Khalil and Rasmussen, 1994; Kazil et al., 2011). An SO_2 flux of $1.0\,pptv\,h^{-1}$ was included in order to represent the processes associated with dimethyl sulphide, in lieu of an explicit scheme (Gray et al., 2011; Yang et al., 2011).

The wet deposition scheme used does not allow for re-suspension of aerosols during the evaporation of rain droplets and hence is likely to lead to an overly strong aerosol sink (Saide et al., 2011).

The horizontal domain size was $9\,km \times 9\,km$ with grid cell resolution of $300\,m$. The model extends $1.5\,km$ vertically, with 50 vertical layers (increasing in depth with height). Each control case was simulated for $35\,h$, starting at 22:00:00 local time (LT) on 21 July 2001. The sun rose at 05:20:00 LT, and set at 19:00:00 LT. Control case results are presented inclusive of the spin-up period. The choice of relatively coarse horizontal resolution follows Wang and Feingold (2009a) and has been used in subsequent modelling studies (Chen et al., 2011; Wang et al., 2011). The relatively small horizontal domain size allows detailed analysis of the aerosol injection and aerosol interaction with clouds, with computational expediency. Analysis of the post-injection simulations is limited to the five hour period subsequent to injection. After this time, the domain becomes saturated with aerosols that would otherwise be advected over a larger domain size. Larger scale feedbacks, as considered in other cloud-resolving investigations (Wang and Feingold, 2009a; Wang et al., 2009) are outside the scope of this work.

3 Experimental design

For each of the three background aerosol concentrations, four aerosol injection simulations were performed, corresponding to aerosol injection in the early morning (03:00:00 LT), mid-morning (08:00:00 LT), day (13:00:00 LT) and evening (18:00:00 LT). These times represent injection into the various conditions of the diurnally varying MSc. Additional experiments investigated the effects of varying the aerosol injection rate and were carried out for weakly precipitating conditions only.

The spraying vessel was assumed to travel the length of the 9 km domain once, along the middle of the domain, at a speed of $5\,\mathrm{m\,s^{-1}}$. This moving aerosol injection was simulated as an increase in Na and Cl aerosol in one base-layer grid cell at a time. The mass and number fluxes were based on injection rates estimated by Salter et al. (2008) with an injection rate of $30\,\mathrm{kg\,s^{-1}}$ of sea water forming a wet spray of 800 nm diameter. As such, these aerosols were emitted into the third size bin (representing a dry diameter of 200 nm). The mass flux of Na was $4436\,\mathrm{\mu g\,m^{-2}\,s^{-1}}$, the mass flux of Cl was $6840\,\mathrm{\mu g\,m^{-2}\,s^{-1}}$ and the number flux was $1.24 \times 10^{12}\,\mathrm{m^{-2}\,s^{-1}}$. In preliminary testing, it was found that injections greater than half of Salter's full emission rate resulted in unphysical outputs from the SW radiation scheme, ultimately leading to simulation failure. Thus, the maximum injection rate tested had half the mass and number fluxes of the Salter proposed emission (denoted as SA0.5). Experiments to investigate the effects of varying the aerosol injection rate on the weakly precipitating case consisted of injecting a quarter of the Salter injection rate (SA0.25) and a tenth of the Salter rate (SA0.1) at each of the four times through the diurnal cycle. The aerosol injection experiments are summarised in Table 1.

4 Results

Of the three background aerosol concentrations, the pristine marine conditions of the Southern Ocean produced a weakly precipitating case (WP). The North-East Pacific location typical for MSc, and the most heavily polluted East China Sea background aerosol conditions both produced non-precipitating regimes (NP-Pa and NP-Ch, respectively).

4.1 Control cases

4.1.1 Weakly precipitating (WP) control case

This WP control case demonstrated a clear diurnal cycle in both cloud properties (Fig. 1) and dynamical and physical processes (Fig. 2).

Cloud-top LW radiative cooling (Fig. 2c) produced a band of negative buoyancy atop positive cloud layer buoyancy (Fig. 2d). This negative buoyancy produced turbulent kinetic energy (TKE) (Fig. 2e, f) which led to boundary layer mixing (suggested by the vertical velocity variance, Fig. 2a). The SW radiation, present during the day, offset this cloud-top cooling, reducing the TKE and mixing through the boundary layer. The reduced vertical transport of moisture from the surface was evident in an accumulation of total water mixing ratio at the surface during the day (Fig. 2g). As the SW radiation dissipated into the second night, the TKE recovered, allowing improved mixing within the boundary layer. This periodicity in the strength of dynamical and physical processes was reflected in the pattern of cloud properties. During the more turbulent night (and outside of the spin-up period), cloud fraction reached 70 % (Fig. 1e), LWP reached 50 g m^{-2} (Fig. 1c) and the cloud was approximately 400 m deep (Fig. 1b). In these conditions, the low N_d of around 10 cm^{-3} produced precipitation (Fig. 1a, d). The peak surface precipitation rate was 0.6 mm day^{-1}, whilst the cloud base rate at this time was nearly 1.2 mm day^{-1} (Fig. 1d). The domain average calculated cloud albedo reached 0.35 during the night (Fig. 1f). During the daytime, cloud fraction and LWP both fell to zero as the cloud dissipated in the less turbulent conditions. As such, precipitation and albedo also fell to zero. For this WP case, there was a period of approximately 6 h during the day between cloud dissipation and cloud recovery.

Even during the night, the cloud and boundary layers were not well coupled. Turbulence was largely confined to the cloud layer, as was vertical velocity variance, and the boundary layer became stratified (Fig. 2g). Additionally, over the 35 h long control

simulation, both cloud top and cloud base heights decreased (by around 350 m and 300 m, respectively).

4.1.2 Non-precipitating (NP) control cases

Similar to the WP case, the NP cases also showed clear diurnal patterns in cloud properties (Fig. 3) and physical and dynamical processes (Fig. 4).

The background aerosol concentration initialisations led to cloud average N_d of almost 200 cm^{-3} for NP-Pa and around 500 cm^{-3} for NP-Ch case. In both cases, the N_d was sufficient to inhibit precipitation formation (Fig. 3d).

As in the WP case, LW cloud-top radiative cooling (Fig. 4c) produced a band of negative buoyancy at the cloud top (Fig. 4d) that resulted in TKE (Fig. 4e, f). Cloud-top radiative cooling was stronger in the NP case than in the WP case, resulting in a stronger vertical velocity variance (Fig. 4a) and a better mixed/less stratified boundary layer (Fig. 4g). Whilst SW radiation during the day again heated the clouds (subduing cloud-top LW radiative cooling and negative buoyancy) they did not fully dissipate. Thus, although weakened during the day, these dynamical and physical processes were maintained over the diurnal cycle.

The diurnal cycle was again seen in the cloud properties. Unlike the total loss of LWP during the day seen in the WP case, the minimum LWP for both of the NP cases was approximately 10 g m^{-2}. This recovered to around 35 g m^{-2} (NP-Pa) and 30 g m^{-2} (NP-Ch) during the subsequent night (Fig. 3c). Similarly, whereas the daytime cloud fraction in the WP case fell to zero, in the NP cases this minimum was maintained at 15 % for NP-Pa, and 5 % for NP-Ch, recovering to 90 % for both cases into the night (Fig. 3e). Cloud was also maintained at a higher fraction for longer, with slower dissipation into the day, and a shorter period of low cloud fraction. Owing to the inverse relationship between cloud droplet radius and optical thickness, the higher cloud average N_d for NP-Ch caused the domain average calculated cloud albedo to be consistently higher than the NP-Pa case, despite the lower cloud fraction and LWP values (Fig. 3f). This

cloud albedo also showed a diurnal cycle, ranging from approximately 0.35 to 0.6 for the day and night time values in NP-Ch and from approximately 0.3 to 0.5 for NP-Pa.

Cloud-top height decreased by 150 m over the 35 h simulation, with the decrease being more exaggerated during the day as turbulence levels decrease. There was additionally a diurnal cycle in cloud base height, with the base rising during the day, causing cloud thinning to around 100 m. The cloud doubled in thickness during the night. These cloud height properties were similar for both NP cases.

Whilst there were some similarities between processes in the WP and NP clouds (albeit of differing strength), one area of disparity was the vertical velocity skewness – a measure of the relative strengths of updrafts and downdrafts (Figs. 2b, 4b). In the NP control cases, strong downdrafts driven by the cloud top LW radiative cooling descended towards the surface, producing a negative skewness throughout the boundary layer. This was in contrast to the WP case, which showed positive skewness within the cloud layer, and negative skewness below.

The diurnal patterns shown in the control cases were similar to previous simulations of the diurnal cycle in marine stratocumulus. For example, LWP magnitudes were similar to those achieved in the simulations of Wang and Feingold (2009a), Wang et al. (2011), and Chen et al. (2011). Whilst the LWP magnitudes were lower than the range of measurements in the DYCOMS-II (RF02) case (90 to 120 g m^{-2}), on which the input soundings of these simulations were based, it is noted that the DYCOMS-II measurements assume an average over open and closed cells, and aerosol concentrations differ from the observed conditions. Other features of the control cases suggest typical MSc behaviour. Negative vertical velocity skewness in the NP cases, peaking in the lower third of the boundary layer, agrees with the observations of Hogan et al. (2009). The positive skewness within the cloud in the WP case being consistent with wide downward motions associated with droplet sedimentation within the cloud (Ackerman et al., 2009) and strong, narrow downdrafts, associated with precipitation below the cloud (Wang and Feingold, 2009a). Additionally, the stratification observed

The effects of marine cloud brightening aerosol injection on albedo changes

A. K. L. Jenkins et al.

Title Page

Abstract	Introduction
Conclusions	References
Tables	Figures

◄◄   ►►

◄   ►

Back   Close

Full Screen / Esc

Printer-friendly Version

Interactive Discussion

in the total water mixing ratio of the WP case suggests uncoupling of the cloud and boundary layers (Jones et al., 2011b) which is typical of precipitating MSc.

4.2 The effect of aerosol injection

The effects of aerosol injection on albedo were considered by three measures.

1. ($\Delta\alpha_{CC}$) The change in domain average cloud albedo for times of SW radiation in the 5 h subsequent to injection compared to the control. This uses the simplified calculation of Twomey (1977) for optical cloud thickness, $\tau = 2\pi N\bar{r}^2 h$, where N is the drop concentration, $\bar{r}$ = a representative mean radius calculated from the mass of liquid water and droplet concentration at each grid cell, and h is the depth of the grid cell. This was then converted into albedo (A) using the approximation, $A = \tau/(6.8 + \tau)$ (Lacis and Hansen, 1974; Zhang et al., 2005). An estimation of the aerosol effect on cloud albedo in the absence of LWP increase was also included (i.e. a fixed LWP assumption, $\Delta\alpha_{CC\_fixed\_LWP}$), whereby the calculation was repeated with control case LWP and increase in N_d weighted for this control case LWP.

2. ($\Delta\alpha_{AS}$) The domain average change in all-sky planetary albedo for times of SW radiation in the 5 h subsequent to injection compared to the control was calculated as the ratio of upward to downward SW radiation at the top of atmosphere. This incorporates the concurrent effects of both cloud albedo change and direct aerosol effects.

3. ($\Delta\alpha_{CS}$) The domain average change in clear-sky albedo for times of SW radiation in the 5 h subsequent to injection compared to the control was calculated. Since this is calculated in the absence of clouds, and therefore neglects the masking effect of overlying clouds, $\Delta\alpha_{CS}$ is a measure of the maximum direct aerosol effect.

Since the brightening of clouds is only effective at producing a negative radiative perturbation during daylight, all measures of albedo were calculated only when downward

The effects of marine cloud brightening aerosol injection on albedo changes

A. K. L. Jenkins et al.

SW radiation is present. As such, the early morning and evening injection times have a reduced analysis period. Injection into the early morning captures the latter portion of cloud alterations, while the injection into the evening captures only 40 min after the beginning of injection.

4.2.1 Aerosol injection into WP case

We initially consider the response of the WP case to SA0.5 injection of aerosol at the four different points during the diurnal cycle.

The cloud average N_d increased in response to injection at all four times during the diurnal cycle. This increase ranged from a five-fold increase (to $117 \, \text{cm}^{-3}$) for injection into the low cloud fraction during the day (13:00:00 LT), to an increase of almost 17 times the original concentration (to $234 \, \text{cm}^{-3}$) for injection in the mid-morning (08:00:00 LT) (Table 2). These N_d increases were sufficient to reduce the domain mean precipitation rate by up to 88 % averaged over the time where SW radiation was present in the 5 h subsequent to injection. However, no change occurred for injection into the cloud-free day at which time background precipitation has already ceased, or for evening injection (18:00:00 LT) where precipitation rates had not yet recovered. The precipitation decreases produced an increase in LWP compared to the control case of 43 % for early morning injection (03:00:00 LT), and 114 % for mid-morning injection. In addition to LWP increases, injecting aerosols into cloudy conditions resulted in an increase in cloud fraction. Early morning injection doubled the cloud fraction while mid-morning injection tripled the cloud fraction. The cloud fraction, and associated perturbations were negligible for day and evening injections. Aerosol injection also affected the cloud height, particularly when injected into the dissipating cloud in the early and mid mornings. Here, the cloud top descent seen in the control case was replaced by cloud top height maintenance (Fig. 5). A slight cloud top increase was also seen for evening injection, although as this is into the post-SW growth phase of the cloud, the perturbation is less marked. Again, no cloud changes occurred when injecting into the cloud-free day.

Considering how these changes to cloud properties are related to albedo, Fig. 6 shows the $\Delta\alpha_{CC}$, $\Delta\alpha_{AS}$ and $\Delta\alpha_{CS}$ for an aerosol injection rate of SA0.5. There is a clear variation in the $\Delta\alpha_{CC}$ response for aerosol injections at different times during the diurnal cycle. Early and mid morning injections produced the largest $\Delta\alpha_{CC}$ of 0.28 and 0.17, respectively. As the cloud recovered into the second night, evening injection produced a slight $\Delta\alpha_{CC}$ of 0.01. Whilst there was also a clear variation in both the $\Delta\alpha_{AS}$ and $\Delta\alpha_{CS}$ responses for aerosol injection at different times during the diurnal cycle, the pattern was different to that seen in cloud response only. The largest $\Delta\alpha_{AS}$ was seen for early morning injection at 0.11, decreasing to 0.06 for mid-morning injection, and decreasing further for evening injection at 0.04. The clearest of the deviations from the $\Delta\alpha_{CC}$ pattern was during the cloud-free day, where the $\Delta\alpha_{AS}$ was 0.06. The $\Delta\alpha_{AS}$ was matched by the $\Delta\alpha_{CS}$ response at this time, indicating that the $\Delta\alpha_{AS}$ was purely from the direct aerosol effect. The vertical distribution of the domain maximum unactivated aerosol concentration is shown for each injection time in Fig. 7. The $\Delta\alpha_{CS}$ also increased the $\Delta\alpha_{AS}$ more than the $\Delta\alpha_{CC}$ did for the evening injection where cloud fraction was low. The $\Delta\alpha_{CS}$ again showed a different diurnal pattern. Early morning injection again produced the largest perturbation of 0.08, falling to 0.04 for injection in the mid-morning. This recovered into the day, producing a $\Delta\alpha_{CS}$ of 0.07. The response was again low for evening injection, producing a $\Delta\alpha_{CS}$ of 0.02.

4.2.2 Aerosol injection into NP cases

Injection into the NP cases resulted in larger absolute N_d increases than in the WP case (Table 3). Increases were also generally larger for the less polluted NP-Pa case than the more polluted NP-Ch case. The maximum resulting domain and time averaged N_d following injection ranged from $234\,cm^{-3}$ (WP) to $315\,cm^{-3}$ (NP-Pa) and $632\,cm^{-3}$ (NP-Ch). These values decreased for injection at the least effective times of day to $117\,cm^{-3}$, $179\,cm^{-3}$ and $517\,cm^{-3}$, respectively. It is noted that these averages are for a small domain size, in the time immediately after injection and should therefore be larger than those obtained in longer time scale and larger domain size simulations.

This is true when comparing to the finding of Wang et al. (2011), who report average N_d of $65\,mg^{-1}$ and $46\,mg^{-1}$ for their precipitating cases (where $1\,mg^{-1}$ is equal to $1\,cm^{-3}$ for an air density of $1\,kg\,m^{-3}$). As there was no precipitation to prevent, no precipitation change occurred (Table 2). The LWP changes were small (up to 2 %), with small losses during the NP-Ch morning. Cloud fraction, cloud top and cloud base heights all showed negligible perturbations. Whilst the magnitudes of $\Delta\alpha_{CC}$ were generally significantly smaller for the NP cases compared to the WP cases, these were also sensitive to the timing of injection. For NP-Pa no perturbation was produced for mid-morning injection, although a $\Delta\alpha_{CC}$ of 0.04 resulted from early morning injection. This peak value was only 13 % of the maximum $\Delta\alpha_{CC}$ reached when injecting into the WP cloud. For the more heavily polluted NP-Ch case, the pattern was repeated, although where $\Delta\alpha_{CC}$ occur, the magnitude was less than half that of the NP-Pa case.

The $\Delta\alpha_{AS}$ was similarly significantly lower than for the WP case. The maximum $\Delta\alpha_{AS}$ obtained for the NP cases occurred for injection into the day (0.02) and was around a sixth of that achieved in the WP case. The values of $\Delta\alpha_{AS}$ were similar for both NP cases. The $\Delta\alpha_{CS}$ followed the same alternating pattern as that of the WP case, with higher perturbations in the early morning and day.

4.2.3 Rate of aerosol injection into WP case

For early and mid morning injection into the WP case, N_d increased with injection rate. However, the relationship was non-linear and tended to flatten at higher aerosol injection rates (Table 3). The opposite relationship occurred for day and evening injections, with decreasing N_d as aerosol injection rates increased. Precipitation rates were uniformly reduced across all injection rates for the early and mid-morning. The LWP showed small increases with aerosol injection rates for the early and mid morning injection times, as did the cloud fraction. The $\Delta\alpha_{CC}$ also increased with increasing aerosol injection rates for both the early and mid morning injections (Fig. 8). This relationship was non-linear, showing a flattening gradient at higher aerosols injection rates. For example, the rate of $\Delta\alpha_{CC}$ increase with respect to increase in injection rate reduced to

a third for the higher injection rates (SA0.25 to SA0.5) into the cloud in the mid-morning compared to the lower injection rates (SA0.1 to SA0.25). This reduction was just under a half for injection into the early morning cloud. Injecting into the cloud-free conditions of the WP day produced no $\Delta\alpha_{CC}$, regardless of aerosol concentration. Increasing the

5 injection rate between SA0.1 and SA0.5 also had little effect on $\Delta\alpha_{CC}$ when injecting into the recovering evening cloud.

The effect of increasing the aerosol injection rates on $\Delta\alpha_{AS}$ also varied through the diurnal cycle. The $\Delta\alpha_{AS}$ showed a positive correlation with increasing injection for early and mid morning injection. Again, the rate of $\Delta\alpha_{AS}$ increase with injection rate was

10 non-linear, the gradient of the response typically halving for the higher injection rates. This relationship was again weaker for the evening, with little variation in the $\Delta\alpha_{AS}$ for different injection rates. The $\Delta\alpha_{CS}$ again showed a non-linearly increasing response.

5 Discussion

Whilst both the NP and WP regimes demonstrate the first indirect aerosol effect

15 (Twomey, 1977), only the WP regime demonstrates the second indirect aerosol, or "lifetime", effect (Albrecht, 1989). This can be estimated as the difference between $\Delta\alpha_{CC}$ and $\Delta\alpha_{CC\_fixed\_LWP}$ (Fig. 6). It can be seen that this second indirect aerosol effect is only significant when aerosols are injected into precipitating clouds (in the early and mid morning of the WP regime). In these conditions, the second indirect aerosol effect is

20 more effective at increasing the $\Delta\alpha_{CC}$ than the first indirect effect, in agreement with Wang et al. (2011). As such, there is no significant second indirect aerosol effect when injecting into the cloud-free day, or into the evening where the cloud is in a period of re-growth and has not recovered sufficiently for precipitation. Whilst increases in LWP, and hence the presence of the second indirect aerosol effect agrees with ship track obser-

25 vations carried out by Christensen and Stephens (2011), the magnitude of the second indirect aerosol effect will be highly dependent upon conditions, including cloud base height and precipitation rates (Wood, 2007; Wang et al., 2011). Although differences

exist between the cause of ship tracks and proposed cloud brightening methods, they serve as a useful observable analogy to the aerosol enhancement process.

The albedo response for the NP regime is significantly lower than for the WP regime, in agreement with the results of Wang et al. (2011). The LWP changes in the NP case are small. Slight LWP losses for early and mid morning aerosol injections in the NP-Ch case suggests increased evaporation of the now smaller cloud droplets. These findings agree with LWP losses found by Christensen and Stephens (2011) in observations of ship tracks through closed cell regimes.

Changes in cloud properties suggest that the injected WP cloud is undergoing a regime change to a more persistent, non-precipitating cloud type. In addition to increases in LWP, the cloud-top height is maintained (in place of control case cloud-top height decrease) for injection into the early and mid morning, and the clouds persist into the day. The cloud top height increases are again consistent with those observed by Christensen and Stephens (2011) for ship tracks in the precipitating, open cellular regimes. The indication of regime change is also evident in changes to the vertical velocity skewness as the positive cloud-top skewness of the control case becomes more negative after injection (Fig. 5b). The effectiveness of this morning injection is consistent with the hypothesis proposed by Wang et al. (2011). Whilst the immediate impact of aerosol injection into the clouds in the evening is reduced owing to the lack of SW radiation, regime change may continue through the night, persisting into the subsequent day. Indicators of regime change do not occur for injection into the cloud-free day, regardless of aerosol injection rate. Turbulence is low, and supersaturation is below that needed for droplet activation, although future droplet activation may occur during the subsequent more turbulent night. No indicators of regime change occur for aerosol injection at any time into the NP regime. It is noted that the magnitudes of the regime change indicators in all cases will be sensitive to dynamic feedbacks at larger scales (Wang and Feingold, 2009b). The sensitivity of all-sky planetary albedo change to aerosol injection time during the diurnal cycle – particularly for the weakly precipitating regime – suggests that studies that omit this feature may overestimate

The effects of marine cloud brightening aerosol injection on albedo changes

A. K. L. Jenkins et al.

Title Page

Abstract	Introduction
Conclusions	References
Tables	Figures

|◄ | ►|

◄ | ►

Back | Close

Full Screen / Esc

Printer-friendly Version

Interactive Discussion

all-sky planetary albedo increases (although the presence of a direct aerosol effect at cloud-free times would ameliorate this).

The non-linear effect of the rate of aerosol injection on planetary albedo changes in the WP case suggests that an asymptotic limit in increasing the $\Delta\alpha_{AS}$ may lie above SA0.5 (Fig. 8). Injection rates greater than SA0.5 led to unphysical model outputs and simulation failure. This demonstrates that the large aerosol fluxes proposed in order to cover large areas of the ocean produce an extreme response if emitted from a point source. The effects of these locally high aerosol concentrations prior to dispersion are not considered in the uniform aerosol application assumed in global models.

The disparities between calculated $\Delta\alpha_{CC}$ and $\Delta\alpha_{AS}$ in the WP case for early and mid-morning injections (Figs. 6, 8) suggests that the large $\Delta\alpha_{CC}$ are not being fully achieved in the planetary albedo response. It is suggested that the high concentration of aerosols emitted via the point source injection technique contribute towards this disparity through an offsetting/tempering effect. Figure 7 shows high concentrations of unactivated injected aerosol that have penetrated through the cloud in the early/mid morning and evening WP cases. These aerosols accumulate in a layer above the cloud top. The sea-salt aerosols modelled here are non-absorbing and highly scattering. Whilst these would therefore typically not be associated with SW attenuation, radiative transfer modelling of atmospheric concentrations of non-absorbing sea-salt aerosol overlying a surface albedo of 0.1 have produced a positive SW forcing at the tropopause of up to $+5\,\mathrm{W\,m^{-2}}$ (Li et al., 2008). This occurs at solar zenith angles up to 30° (equivalent to between 10:00:00 LT and 14:00:00 LT in our simulations). In this range, the predominantly forward scattering of the sea-salt aerosols causes the majority of the SW radiation to reach the surface. The reflected SW radiation is then reduced through near-infrared absorption, which for sea-salt particles is stronger relative to the absorption in the ultra-violet/visible range (Hatzianastassiou et al., 2007). Attenuation of upward radiation may also result from increases in total water mixing ratio above the cloud top (Fig. 5d), associated with the transported aerosols. The presence of absorbing material in the sea-salt aerosol would exacerbate the effect, with previous

Title Page

Abstract | Introduction

Conclusions | References

Tables | Figures

◄ | ►

◄ | ►

Back | Close

Full Screen / Esc

Printer-friendly Version

Interactive Discussion

modelling and observational studies showing that partially absorbing aerosols over-lying clouds reduce the measured upward irradiance and hence produce low biases in satellite retrievals of cloud optical depth (Haywood et al., 2004; Coddington et al., 2010). A radiatively positive effect was also shown in the modelling of mildly absorb-ing organic aerosols internally mixed in sea-salt aerosols at mass fractions as low as 10 % (Randles et al., 2004). Future radiative transfer modelling of the unnaturally high sea-salt aerosol concentrations that would be present during cloud brightening, and the impact of their vertical position relative to clouds, is suggested.

The apparent offsetting/tempering role of the direct effect increases with increasing injection rate, demonstrated by the increasing disparity between $\Delta\alpha_{CC}$ and $\Delta\alpha_{AS}$ in the early and mid morning cases (Fig. 8). However, this is not sufficient to overcome the increasing $\Delta\alpha_{CC}$ and $\Delta\alpha_{AS}$ with aerosol injection rate (Fig. 8). As simulations carried out at the global scale are unable to represent the locally high aerosol concentrations associated with an aerosol point source, they are unable to simulate this effect.

6 Conclusions

Simulations were carried out using a cloud-resolving model at small domain size. These were used to investigate the detailed response of MSc cloud systems to the in-jection of aerosols at different times during the diurnal cycle, and to the effects and inter-actions of the direct aerosol effect resulting from the concentrated injection of aerosols from a point source.

Based on these simulations, the optimal point in the diurnal cycle for all-sky plan-etary albedo response is early morning injection into the weakly precipitating cloud regime. This results from a large second indirect aerosol effect and cloud conversion towards the more persistent non-precipitating regime. Whilst the direct aerosol effect increases all-sky planetary albedo during the cloud-free day, the lack of cloud changes suggests that this enhancement may be shorter-lived. Injecting aerosols from a point source leads to penetration and accumulation of unactivated aerosols above the cloud.

The direct effect of these overlying aerosols appears to mask (or temper) increases in cloud albedo. Future cloud-resolving modelling, at larger domain sizes and over longer analysis periods could capture the potential tempering effects, along with the complex dynamical feedbacks associated with MSc. These simulations could also be used to
5 quantify the persistence of clouds after aerosol injections.

In any discussion of the effectiveness of geoengineering in altering climate properties, it is necessary to emphasize the importance of the concomitant examination of ethical validity and governance. However, debate and decision-making must be informed by realistic model simulations, particularly given the strict limitations imposed
10 on field testing. The development of realistic model simulations involves the representation of physical implementation details, particularly those that might act to limit the scheme's effectiveness. Here, the all-sky planetary albedo was found to be sensitive to both the timing of the injection with respect to the cloud diurnal cycle and the high concentration of aerosol resulting from point source emission. Both of these would oc-
15 cur should a single injection vessel be used to cover a large area of cloud. The results suggest that omitting either of these details may lead to overestimates of the achievable increase in all-sky planetary albedo. The results presented here therefore have implications on both the future design of model simulations, and may also inform the development of potential implementation strategies.

References

Abdul-Razzak, H. and Ghan, S. J.: A parameterization of aerosol activation 2. Multiple aerosol types, J. Geophys. Res., 105, 6837–6844, doi:10.1029/1999jd901161, 2000.

Ackerman, A. S., vanZanten, M. C., Stevens, B., Savic-Jovcic, V., Bretherton, C. S., Chlond, A., Golaz, J.-C., Jiang, H., Khairoutdinov, M., Krueger, S. K., Lewellen, D. C., Lock, A., Moeng, C.-H., Nakamura, K., Petters, M. D., Snider, J. R., Weinbrecht, S., and Zulauf, M.: Large-Eddy Simulations of a Drizzling, Stratocumulus-Topped Marine Boundary Layer, Mon. Weather Rev., 137, 1083–1110, doi:10.1175/2008MWR2582.1, 2009.

Albrecht, B. A.: Aerosols, Cloud Microphysics, and Fractional Cloudiness, Science, 245, 1227–1230, doi:10.1126/science.245.4923.1227, 1989.

Bretherton, C. S., Uttal, T., Fairall, C. W., Yuter, S. E., Weller, R. A., Baumgardner, D., Comstock, K., Wood, R., and Raga, G. B.: The Epic 2001 Stratocumulus Study, B. Am. Meteorol. Soc., 85, 967–977, doi:10.1175/BAMS-85-7-967, 2004.

Chen, Y. C., Xue, L., Lebo, Z. J., Wang, H., Rasmussen, R. M., and Seinfeld, J. H.: A comprehensive numerical study of aerosol-cloud-precipitation interactions in marine stratocumulus, Atmos. Chem. Phys., 11, 9749–9769, doi:10.5194/acp-11-9749-2011, 2011.

Christensen, M. W. and Stephens, G. L.: Microphysical and macrophysical responses of marine stratocumulus polluted by underlying ships: Evidence of cloud deepening, J. Geophys. Res., 116, D03201, doi:10.1029/2010jd014638, 2011.

Coddington, O. M., Pilewskie, P., Redemann, J., Platnick, S., Russell, P. B., Schmidt, K. S., Gore, W. J., Livingston, J., Wind, G., and Vukicevic, T.: Examining the impact of overlying aerosols on the retrieval of cloud optical properties from passive remote sensing, J. Geophys. Res., 115, D10211, doi:10.1029/2009jd012829, 2010.

Collins, W. D., Rasch, P. J., Boville, B. A., Hack, J. J., McCaa, J. R., Williamson, D. L., Kiehl, J. T., Briegleb, B., Bitz, C., Lin, S.-J., Zhang, M., and Dai, Y.: Description of the NCAR Community Atmosphere Model (CAM 3.0), NCAR Technical Note, NCAR/TN-464+STR, 2004.

Duynkerke, P. G. and Teixeira, J.: Comparison of the ECMWF Reanalysis with FIRE I Observations: Diurnal Variation of Marine Stratocumulus, J. Climate, 14, 1466–1478, doi:10.1175/1520-0442(2001)014<1466:coterw>2.0.co;2, 2001.

Duynkerke, P. G., de Roode, S. R., van Zanten, M. C., Calvo, J., Cuxart, J., Cheinet, S., Chlond, A., Grenier, H., Jonker, P. J., Köhler, M., Lenderink, G., Lewellen, D., Lappen, C.-l., Lock, A. P., Moeng, C.-H., Müller, F., Olmeda, D., Piriou, J.-m., Sánchez, E., and Sednev, I.:

Observations and numerical simulations of the diurnal cycle of the EUROCS stratocumulus case, Q. J. Roy. Meteor. Soc., 130, 3269–3296, doi:10.1256/qj.03.139, 2004.

Fast, J. D., Gustafson, W. I., Jr., Easter, R. C., Zaveri, R. A., Barnard, J. C., Chapman, E. G., Grell, G. A., and Peckham, S. E.: Evolution of ozone, particulates, and aerosol direct radiative forcing in the vicinity of Houston using a fully coupled meteorology-chemistry-aerosol model, J. Geophys. Res., 111, D21305, doi:10.1029/2005jd006721, 2006.

Fuentes, E., Coe, H., Green, D., de Leeuw, G., and McFiggans, G.: On the impacts of phytoplankton-derived organic matter on the properties of the primary marine aerosol – Part 1: Source fluxes, Atmos. Chem. Phys., 10, 9295–9317, doi:10.5194/acp-10-9295-2010, 2010.

Georgii, H. W. and Gravenhorst, G.: The ocean as source or sink of reactive trace-gases, Pure Appl. Geophys., 115, 503–511, doi:10.1007/bf00876117, 1977.

Gray, B., Wang, Y., Gu, D., Bandy, A., Mauldin, L., Clarke, A., Alexander, B., and Davis, D.: Sources, transport, and sinks of SO_2 over the equatorial Pacific during the Pacific Atmospheric Sulfur Experiment, J. Atmos. Chem., 68, 27–53, doi:10.1007/s10874-010-9177-7, 2011.

Hatzianastassiou, N., Matsoukas, C., Fotiadi, A., P. W. Stackhouse, J., Koepke, P., Pavlakis, K. G., and Vardavas, I.: Modelling the direct effect of aerosols in the solar near-infrared on a planetary scale, Atmos. Chem. Phys., 7, 3211–3229, doi:10.5194/acp-7-3211-2007, 2007.

Haywood, J. M., Osborne, S. R., and Abel, S. J.: The effect of overlying absorbing aerosol layers on remote sensing retrievals of cloud effective radius and cloud optical depth, Q. J. Roy. Meteor. Soc., 130, 779–800, doi:10.1256/qj.03.100, 2004.

Hogan, R. J., Grant, A. L. M., Illingworth, A. J., Pearson, G. N., and O'Connor, E. J.: Vertical velocity variance and skewness in clear and cloud-topped boundary layers as revealed by Doppler lidar, Q. J. Roy. Meteor. Soc., 135, 635–643, doi:10.1002/qj.413, 2009.

Jones, A., Haywood, J., and Boucher, O.: Climate impacts of geoengineering marine stratocumulus clouds, J. Geophys. Res., 114, D10106, doi:10.1029/2008jd011450, 2009.

Jones, A., Haywood, J., and Boucher, O.: A comparison of the climate impacts of geoengineering by stratospheric SO2 injection and by brightening of marine stratocumulus cloud, Atmos. Sci. Lett., 12, 176–183, doi:10.1002/asl.291, 2011a.

The effects of marine cloud brightening aerosol injection on albedo changes

A. K. L. Jenkins et al.

Jones, C. R., Bretherton, C. S., and Leon, D.: Coupled vs. decoupled boundary layers in VOCALS-REx, Atmos. Chem. Phys. Discuss., 11, 8431–8460, doi:10.5194/acpd-11-8431-2011, 2011b.

Kazil, J., Wang, H., Feingold, G., Clarke, A. D., Snider, J. R., and Bandy, A. R.: Modeling chemical and aerosol processes in the transition from closed to open cells during VOCALS-REx, Atmos. Chem. Phys., 11, 7491–7514, doi:10.5194/acp-11-7491-2011, 2011.

Khalil, M. A. K. and Rasmussen, R. A.: Global decrease in atmospheric carbon monoxide concentration, Nature, 370, 639–641, 1994.

Korhonen, H., Carslaw, K. S., and Romakkaniemi, S.: Enhancement of marine cloud albedo via controlled sea spray injections: a global model study of the influence of emission rates, microphysics and transport, Atmos. Chem. Phys., 10, 4133–4143, doi:10.5194/acp-10-4133-2010, 2010.

Lacis, A. A. and Hansen, J.: A Parameterization for the Absorption of Solar Radiation in the Earth's Atmosphere, J. Atmos. Sci., 31, 118–133, doi:10.1175/1520-0469(1974)031<0118:apftao>2.0.co;2, 1974.

Latham, J.: Control of global warming?, Nature, 347, 339–340, 1990.

Latham, J.: Amelioration of global warming by controlled enhancement of the albedo and longevity of low-level maritime clouds, Atmos. Sci. Lett., 3, 52–58, doi:10.1006/asle.2002.0099, 2002.

Lenton, T. M. and Vaughan, N. E.: The radiative forcing potential of different climate geoengineering options, Atmos. Chem. Phys., 9, 5539–5561, doi:10.5194/acp-9-5539-2009, 2009.

Li, J., Ma, X., von Salzen, K., and Dobbie, S.: Parameterization of sea-salt optical properties and physics of the associated radiative forcing, Atmos. Chem. Phys. Discuss., 8, 5813–5845, doi:10.5194/acpd-8-5813-2008, 2008.

Lock, A. P.: The sensitivity of a GCM's marine stratocumulus to cloud-top entrainment, Q. J. Roy. Meteor. Soc., 130, 3323–3338, doi:10.1256/qj.03.114, 2004.

Mann, G. W., Carslaw, K. S., Spracklen, D. V., Ridley, D. A., Manktelow, P. T., Chipperfield, M. P., Pickering, S. J., and Johnson, C. E.: Description and evaluation of GLOMAP-mode: a modal global aerosol microphysics model for the UKCA composition-climate model, Geosci. Model Dev., 3, 519–551, doi:10.5194/gmd-3-519-2010, 2010.

Morrison, H., Curry, J. A., and Khvorostyanov, V. I.: A new double-moment microphysics parameterization for application in cloud and climate models. Part I: Description, J. Atmos. Sci., 62, 1665–1677, doi:10.1175/jas3446.1, 2005.

Title Page

Abstract | Introduction

Conclusions | References

Tables | Figures

◄ | ►

◄ | ►

Back | Close

Full Screen / Esc

Printer-friendly Version

Interactive Discussion

Nieuwstadt, F. T. M. and Duynkerke, P. G.: Turbulence in the atmospheric boundary layer, Atmos. Res., 40, 111–142, doi:10.1016/0169-8095(95)00034-8, 1996.

Partanen, A.-I., Kokkola, H., Romakkaniemi, S., Kerminen, V.-M., Lehtinen, K. E. J., Bergman, T., Arola, A., and Korhonen, H.: Direct and indirect effects of sea spray geoengineering and the role of injected particle size, J. Geophys. Res., 117, D02203, doi:10.1029/2011jd016428, 2012.

Randles, C. A., Russell, L. M., and Ramaswamy, V.: Hygroscopic and optical properties of organic sea salt aerosol and consequences for climate forcing, Geophys. Res. Lett., 31, L16108, doi:10.1029/2004gl020628, 2004.

Rasch, P. J., Latham, J., and Chen, C. C.: Geoengineering by cloud seeding: influence on sea ice and climate system, Environ. Res. Lett., 4, 045112, doi:10.1088/1748-9326/4/4/045112, 2009.

Saide, P. E., Spak, S. N., Carmichael, G. R., Mena-Carrasco, M. A., Howell, S., Leon, D. C., Snider, J. R., Bandy, A. R., Collett, J. L., Benedict, K. B., de Szoeke, S. P., Hawkins, L. N., Allen, G., Crawford, I., Crosier, J., and Springston, S. R.: Evaluating WRF-Chem aerosol indirect effects in Southeast Pacific marine stratocumulus during VOCALS-REx, Atmos. Chem. Phys. Discuss., 11, 29723–29775, doi:10.5194/acpd-11-29723-2011, 2011.

Salter, S., Sortino, G., and Latham, J.: Sea-going hardware for the cloud albedo method of reversing global warming, Philos. T. Roy. Soc. A, 366, 3989–4006, doi:10.1098/rsta.2008.0136, 2008.

Skamarock, W. C., Klemp, J. B., Dudhia, J., Gill, D. O., Barker, D. M., Duda, M. G., Huang, X.-Y., Wang, W., and Powers, J. G.: A Description of the Advanced Research WRF Version 3, NCAR Technical Note, NCAR/TN-475+STR, 2008.

Stevens, B. and Feingold, G.: Untangling aerosol effects on clouds and precipitation in a buffered system, Nature, 461, 607–613, 2009.

Stevens, B., Lenschow, D. H., Vali, G., Gerber, H., Bandy, A., Blomquist, B., Brenguier, J.-L., Bretherton, C. S., Burnet, F., Campos, T., Chai, S., Faloona, I., Friesen, D., Haimov, S., Laursen, K., Lilly, D. K., Loehrer, S. M., Malinowski, S. P., Morley, B., Petters, M. D., Rogers, D. C., Russell, L., Savic-Jovcic, V., Snider, J. R., Straub, D., Szumowski, M. J., Takagi, H., Thornton, D. C., Tschudi, M., Twohy, C., Wetzel, M., and van Zanten, M. C.: Dynamics and Chemistry of Marine Stratocumulus – DYCOMS-II, B. Am. Meteorol. Soc., 84, 579–593, doi:10.1175/BAMS-84-5-579, 2003.

The effects of marine cloud brightening aerosol injection on albedo changes

A. K. L. Jenkins et al.

Title Page

Abstract | Introduction

Conclusions | References

Tables | Figures

|◄ | ►|

◄ | ►

Back | Close

Full Screen / Esc

Printer-friendly Version

Interactive Discussion

Twomey, S.: The Influence of Pollution on the Shortwave Albedo of Clouds, J. Atmos. Sci., 34, 1149–1152, doi:10.1175/1520-0469(1977)034<1149:TIOPOT>2.0.CO;2, 1977.

Wang, H. and Feingold, G.: Modeling Mesoscale Cellular Structures and Drizzle in Marine Stratocumulus. Part I: Impact of Drizzle on the Formation and Evolution of Open Cells, J. Atmos. Sci., 66, 3237–3256, doi:10.1175/2009JAS3022.1, 2009a.

Wang, H. and Feingold, G.: Modeling Mesoscale Cellular Structures and Drizzle in Marine Stratocumulus. Part II: The Microphysics and Dynamics of the Boundary Region between Open and Closed Cells, J. Atmos. Sci., 66, 3257–3275, doi:10.1175/2009JAS3120.1, 2009b.

Wang, H., Skamarock, W. C., and Feingold, G.: Evaluation of Scalar Advection Schemes in the Advanced Research WRF Model Using Large-Eddy Simulations of Aerosol–Cloud Interactions, Mon. Weather Rev., 137, 2547–2558, doi:10.1175/2009MWR2820.1, 2009.

Wang, H., Feingold, G., Wood, R., and Kazil, J.: Modelling microphysical and meteorological controls on precipitation and cloud cellular structures in Southeast Pacific stratocumulus, Atmos. Chem. Phys., 10, 6347–6362, doi:10.5194/acp-10-6347-2010, 2010.

Wang, H., Rasch, P. J., and Feingold, G.: Manipulating marine stratocumulus cloud amount and albedo: a process-modelling study of aerosol-cloud-precipitation interactions in response to injection of cloud condensation nuclei, Atmos. Chem. Phys. Discuss., 11, 885–916, doi:10.5194/acpd-11-885-2011, 2011.

Wood, R.: Cancellation of Aerosol Indirect Effects in Marine Stratocumulus through Cloud Thinning, J. Atmos. Sci., 64, 2657–2669, doi:10.1175/JAS3942.1, 2007.

Yang, M., Huebert, B. J., Blomquist, B. W., Howell, S. G., Shank, L. M., McNaughton, C. S., Clarke, A. D., Hawkins, L. N., Russell, L. M., Covert, D. S., Coffman, D. J., Bates, T. S., Quinn, P. K., Zagorac, N., Bandy, A. R., de Szoeke, S. P., Zuidema, P. D., Tucker, S. C., Brewer, W. A., Benedict, K. B., and Collett, J. L.: Atmospheric sulfur cycling in the Southeastern Pacific – longitudinal distribution, vertical profile, and diel variability observed during VOCALS-REx, Atmos. Chem. Phys. Discuss., 11, 2873–2929, doi:10.5194/acpd-11-2873-2011, 2011.

Zaveri, R. A. and Peters, L. K.: A new lumped structure photochemical mechanism for large-scale applications, J. Geophys. Res., 104, 30387–30415, doi:10.1029/1999jd900876, 1999.

Zaveri, R. A., Easter, R. C., Fast, J. D., and Peters, L. K.: Model for Simulating Aerosol Interactions and Chemistry (MOSAIC), J. Geophys. Res., 113, D13204, doi:10.1029/2007jd008782, 2008.

The effects of marine cloud brightening aerosol injection on albedo changes

A. K. L. Jenkins et al.

Title Page

Abstract	Introduction
Conclusions	References
Tables	Figures

|◄ | ►|

◄ | ►

Back | Close

Full Screen / Esc

Printer-friendly Version

Interactive Discussion

Zhang, Y., Stevens, B., and Ghil, M.: On the diurnal cycle and susceptibility to aerosol concentration in a stratocumulus-topped mixed layer, Q. J. Roy. Meteor. Soc., 131, 1567–1583, doi:10.1256/qj.04.103, 2005.

The effects of marine cloud brightening aerosol injection on albedo changes

A. K. L. Jenkins et al.

Title Page

Abstract | Introduction

Conclusions | References

Tables | Figures

◄ | ►|

◄ | ►

Back | Close

Full Screen / Esc

Printer-friendly Version

Interactive Discussion

Table 1. Aerosol injection experiments. WP indicates aerosol injection into the weakly precipitating control case. NP-Pa and NP-Ch indicate aerosol injection into the non-precipitating cases initialised with aerosol concentrations associated with the North-East Pacific (intermediately polluted) and the East China Sea (heavily polluted), respectively. SA0.5, SA0.25 and SA0.1 describe the aerosol injection rate, as a fraction of the injection rate proposed by Salter et al. (2008).

Time of aerosol injection (LT)	Aerosol injection rate		
	SA0.5	SA0.25	SA0.1
03:00:00	WP	WP	WP
	NP-Pa	–	–
	NP-Ch	–	–
08:00:00	WP	WP	WP
	NP-Pa	–	–
	NP-Ch	–	–
13:00:00	WP	WP	WP
	NP-Pa	–	–
	NP-Ch	–	–
18:00:00	WP	WP	WP
	NP-Pa	–	–
	NP-Ch	–	–

Table 2. Results for the SA0.5 aerosol injection rate. Domain and time-period averaged liquid water path (LWP, $g\,m^{-2}$), cloud fraction (f_c, %), cloud droplet number concentration (N_d, cm^{-3}) and surface rain rate (R_r, $mm\,day^{-1}$). The time average is taken for the times of SW radiation present in the 5 h subsequent to aerosol injection. Percentage perturbation from the control is shown in brackets.

Case	Time of aerosol injection (LT)	LWP $g\,m^{-2}$	f_c %	N_d cm^{-3}	R_r $mm\,day^{-1}$
WP	03:00:00	45.3 (+43 %)	76.3 (+101 %)	176.3 (+1533 %)	0.03 (−88 %)
	08:00:00	15.2 (+114 %)	19.8 (+191 %)	234.3 (+1639 %)	0.05 (−44 %)
	13:00:00	0.5 (0 %)	0.3 (−25 %)	116.9 (+466 %)	0.00 (0 %)
	18:00:00	3.6 (−1 %)	5.6 (0 %)	171.1 (+777 %)	0.00 (41 %)
NP-Pa	03:00:00	60.8 (+2 %)	98.6 (+1 %)	315.0 (+102 %)	0.00 (0 %)
	08:00:00	31.6 (0 %)	79.3 (−1 %)	180.7 (+16 %)	0.00 (0 %)
	13:00:00	14.8 (+1 %)	22.7 (−1 %)	259.8 (+66 %)	0.00 (0 %)
	18:00:00	14.3 (0 %)	22.5 (0 %)	178.8 (14 %)	0.00 (0 %)
NP-Ch	03:00:00	59.1 (−1 %)	98.7 (0 %)	632.2 (+20 %)	0.00 (0 %)
	08:00:00	31.4 (−1 %)	80.3 (−1 %)	517.0 (+1 %)	0.00 (0 %)
	13:00:00	13.7 (+2 %)	19.1 (+2 %)	556.1 (+8 %)	0.00 (0 %)
	18:00:00	11.8 (0 %)	9.1 (+1 %)	528.3 (0 %)	0.00 (0 %)

Table 3. Results for the weakly precipitating (WP) case. Notes as Table 2.

Time of aerosol injection (LT)	Aerosol injection rate	LWP g m^{-2}	f_c %	N_d cm^{-3}	R_r mm day^{-1}
03:00:00	SA0.5	45.3 (+43 %)	76.3 (+101 %)	176.3 (+1533 %)	0.03 (−88 %)
	SA0.25	44.6 (+41 %)	73.0 (+92 %)	141.5 (+1211 %)	0.04 (−85 %)
	SA0.1	44.1 (+39 %)	69.7 (+84 %)	92.9 (+761 %)	0.04 (−82 %)
08:00:00	SA0.5	15.2 (+114 %)	19.8 (+191 %)	234.3 (+1639 %)	0.05 (−44 %)
	SA0.25	14.4 (+106 %)	17.5 (+157 %)	200.3 (+1388 %)	0.05 (−44 %)
	SA0.1	13.1 (+87 %)	14.6 (+118 %)	124.4 (+824 %)	0.06 (−40 %)
13:00:00	SA0.5	0.5 (0 %)	0.3 (−25 %)	116.9 (+466 %)	0.00 (0 %)
	SA0.25	0.5 (0 %)	0.3 (0 %)	134.7 (+553 %)	0.00 (0 %)
	SA0.1	0.5 (0 %)	0.4 (0 %)	181.6 (+780 %)	0.00 (0 %)
18:00:00	SA0.5	3.6 (−1 %)	5.6 (0 %)	171.1 (+777 %)	0.00 (41 %)
	SA0.25	3.6 (−1 %)	5.6 (0 %)	180.6 (+825 %)	0.00 (18 %)
	SA0.1	3.6 (−1 %)	5.6 (0 %)	139.9 (+617 %)	0.00 (4 %)
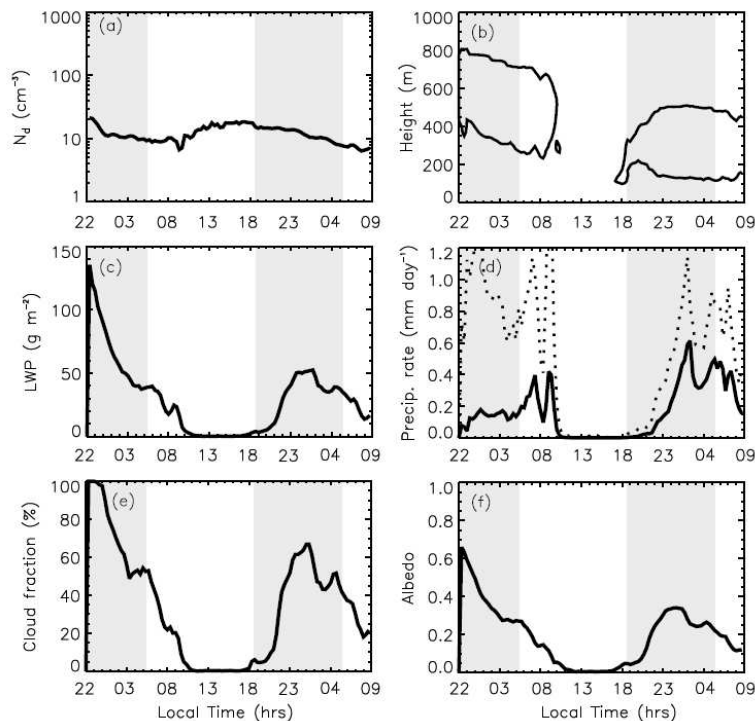
Fig. 1. Time evolution of domain averaged cloud properties for the WP control case. **(a)** Cloud droplet number concentration (N_d, cm^{-3}); **(b)** cloud top and cloud base height (contour at cloud water mixing ratio of $0.01\,\mathrm{g\,kg^{-1}_{dry\ air}}$); **(c)** liquid water path (LWP, $\mathrm{g\,m^{-2}}$); **(d)** surface rain rate (solid), and cloud base rain rate (dotted) ($\mathrm{mm\,day^{-1}}$); **(e)** cloud fraction (%); and **(f)** cloud albedo. Shading indicates the night.
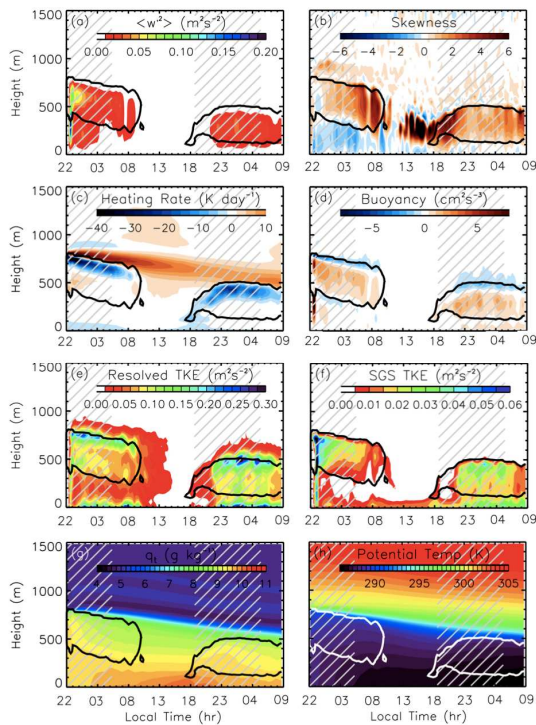
Fig. 2. Time evolution of domain averaged dynamic and physical properties for the WP control case. **(a)** Vertical velocity variance ($< w'^2 >$, $m^2 s^{-2}$); **(b)** vertical velocity skewness; **(c)** radiative heating rate ($K\,day^{-1}$); **(d)** buoyancy ($cm^2 s^{-3}$); **(e)** resolved turbulent kinetic energy ($m^2 s^{-2}$); **(f)** sub-grid scale turbulent kinetic energy ($m^2 s^{-2}$); **(g)** total water mixing ratio ($g\,kg^{-1}_{dry\,air}$); and **(h)** potential temperature (K). Solid lines indicate the cloud top and cloud base height (a contour at cloud water mixing ratio of 0.01 $g\,kg^{-1}_{dry\,air}$). Hatch lines indicates the night.
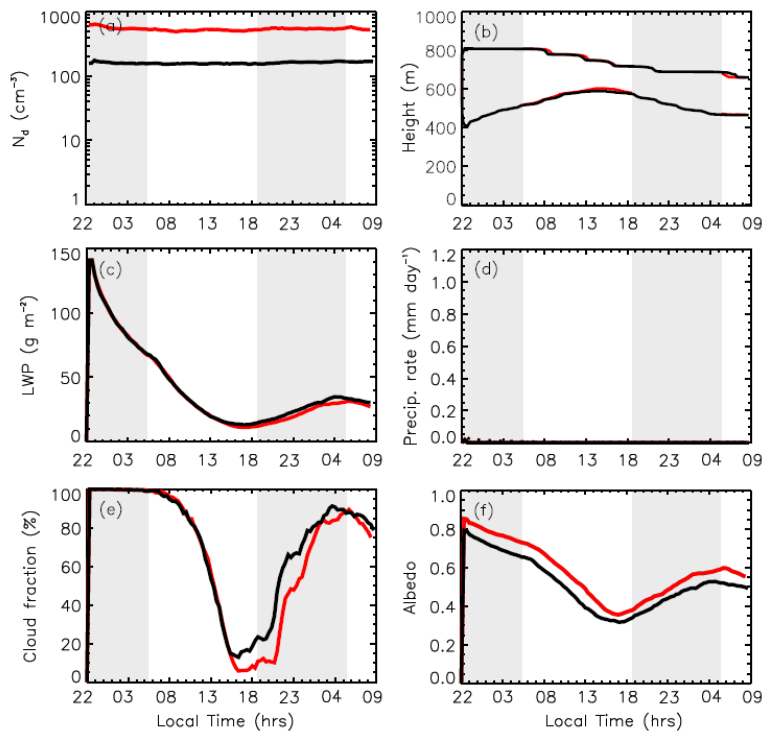
Fig. 3. Time evolution of domain averaged cloud properties for the NP-Ch (red) and NP-Pa (black) cases. Descriptions as Fig. 1.
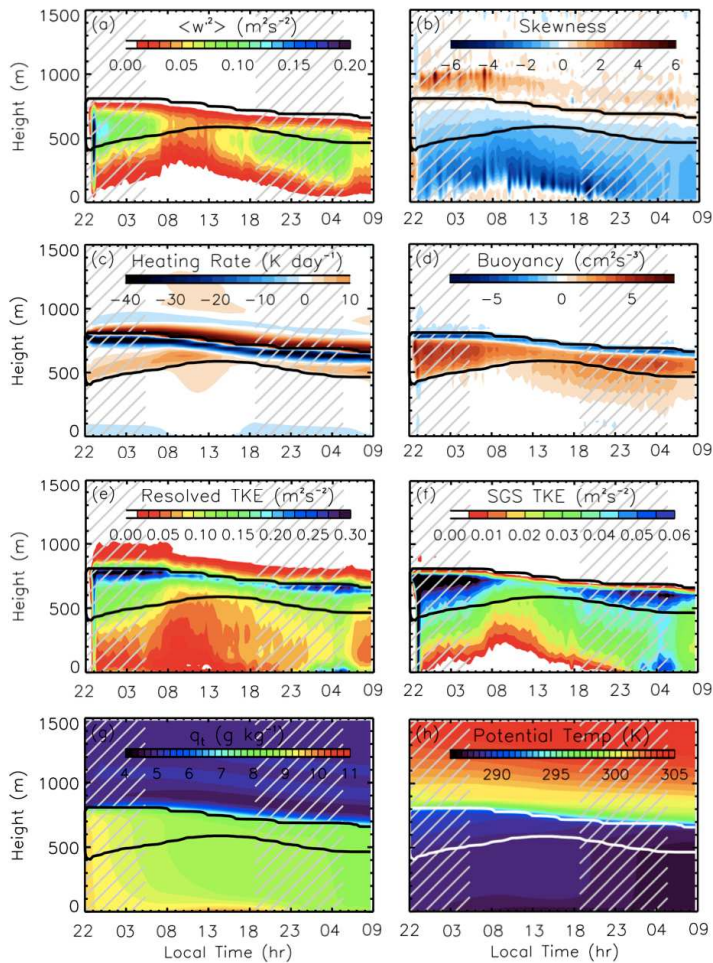
Fig. 4. Time evolution of domain averaged dynamic and physical properties for NP-Pa control case. Descriptions as Fig. 2.

Title Page

Abstract | Introduction

Conclusions | References

Tables | Figures

◄ | ►►

◄ | ►

Back | Close

Full Screen / Esc

Printer-friendly Version

Interactive Discussion
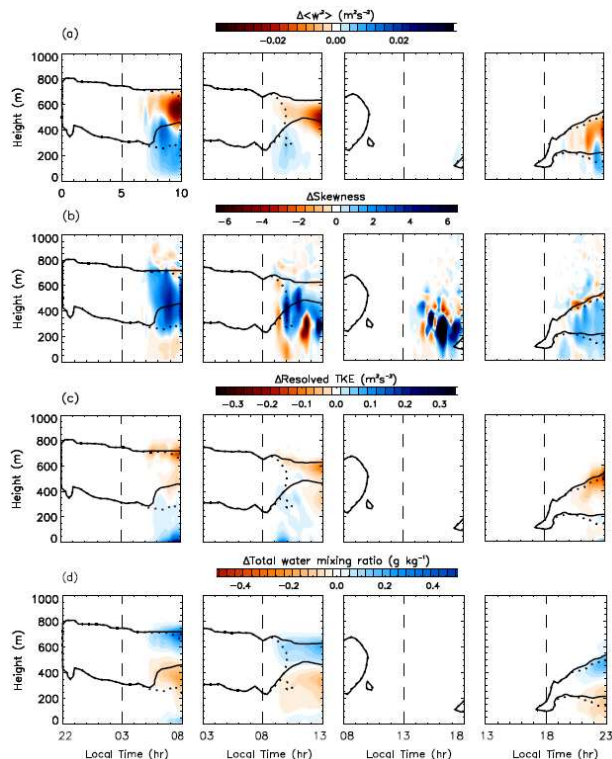
Fig. 5. Time evolution for WP SA0.5 injection-induced perturbations in domain averaged: **(a)** vertical velocity variance ($<w'^2>$, $m^2\,s^{-2}$); **(b)** vertical velocity skewness; **(c)** resolved turbulent kinetic energy ($m^2\,s^{-2}$); and **(d)** total water mixing ratio ($g\,kg_{dry\ air}^{-1}$). Solid lines indicate the perturbed domain average cloud top and base (contour at cloud water mixing ratio of $0.01\,g\,kg_{dry\ air}^{-1}$). Control case domain average cloud top and base are indicated by the dotted lines. The dashed vertical lines indicate the time of aerosol injection.
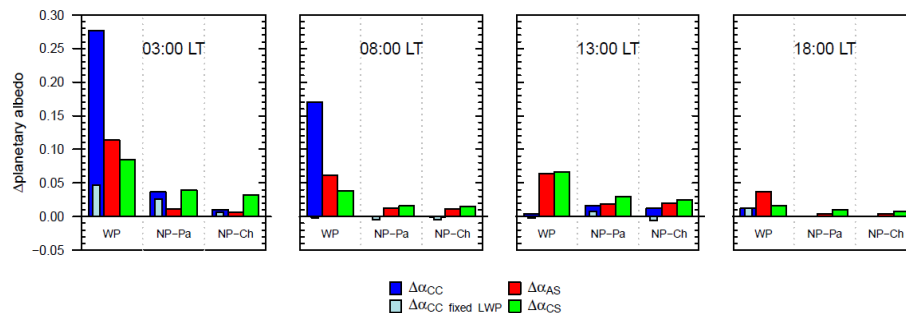
Fig. 6. Domain and time averaged albedo perturbations associated with aerosol injection at the SA0.5 rate, at 03:00:00 LT, 08:00:00 LT, 13:00:00 LT and 18:00:00 LT into the weakly precipitating regime (WP) and non-precipitating regime (NP-Pa and NP-Ch). In each case, four measures of the effects of aerosol injection on albedo perturbations are shown: the change in cloud albedo ($\Delta\alpha_{CC}$); the change in cloud albedo assuming a LWP fixed at the control magnitudes with weighted N_d increases ($\Delta\alpha_{CC\_fixed\_LWP}$); the change in all-sky planetary albedo ($\Delta\alpha_{AS}$); and the change in clear-sky albedo ($\Delta\alpha_{CS}$).
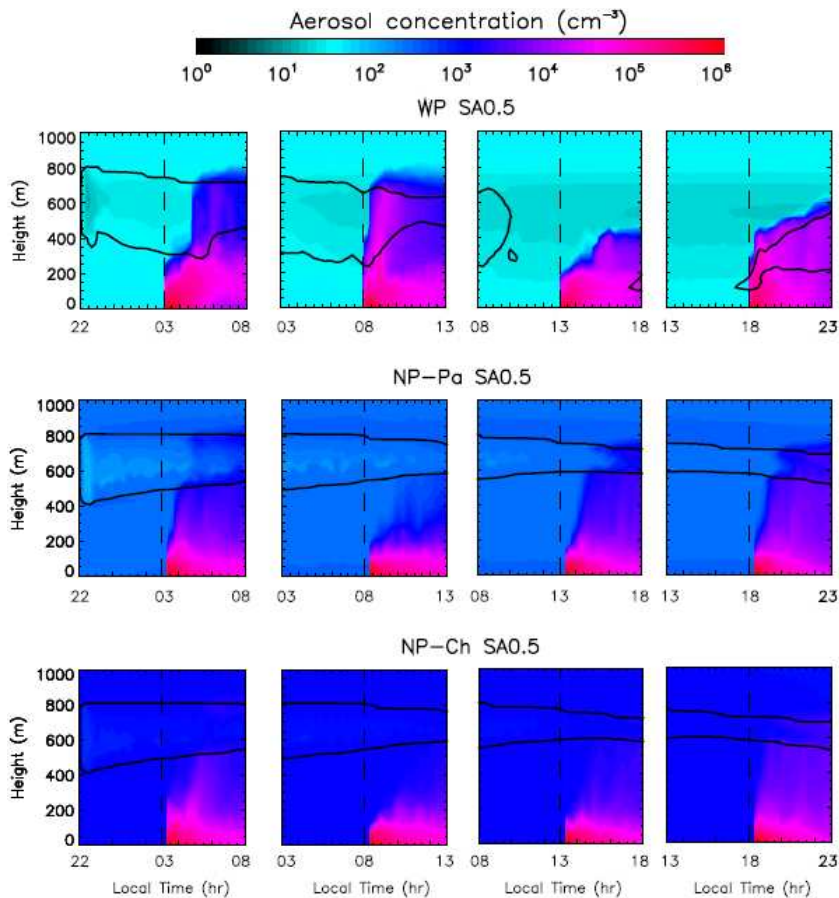
Fig. 7. Time series of domain maximum aerosol concentrations (cm^{-3}) for the WP, NP-Pa and NP-Ch cases (all SA0.5 aerosol injection rate). Plots include 5 h prior to injection and 5 h subsequent to injection, with aerosol injection start time being indicated by the vertical dashed line.

The effects of marine cloud brightening aerosol injection on albedo changes

A. K. L. Jenkins et al.

Title Page

Abstract	Introduction
Conclusions	References
Tables	Figures

|◄ | ►|

◄ | ►

Back | Close

Full Screen / Esc

Printer-friendly Version

Interactive Discussion
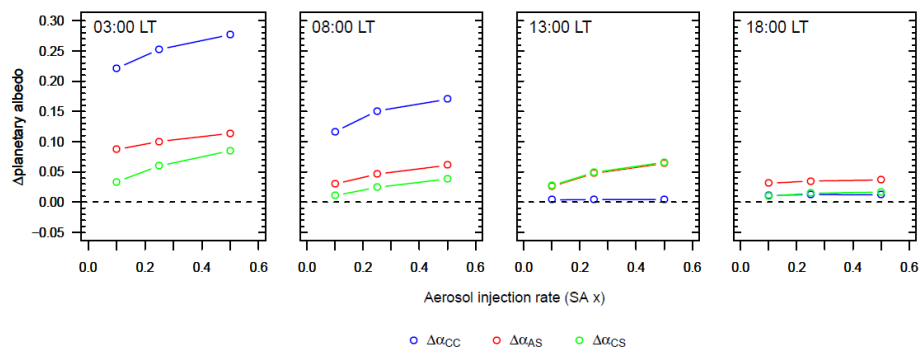
Fig. 8. Domain and time average albedo perturbations associated with SA0.1, SA0.25 and SA0.5 aerosol injection rates at 03:00:00 LT, 08:00:00 LT, 13:00:00 LT and 18:00:00 LT into the weakly precipitating (WP) regime. In each case, three measures of the effects of aerosol injection on albedo perturbations are shown: the change in cloud albedo ($\Delta\alpha_{CC}$); the change in all-sky planetary albedo ($\Delta\alpha_{AS}$); and the change in clear-sky albedo ($\Delta\alpha_{CS}$).